THE JOURNAL OF PHYSICAL CHEMISTRY C

C: Energy Conversion and Storage; Energy and Charge Transport

Creation of Acceptor Centers in ZnO Single Crystals by Annealing in Sb Vapor

Nikolai O. Taibarei, Vladimir G Kytin, Eugenii E. Kupriyanov, Vladimir A. Kulbachinskii, Maksim A. Makhiboroda, and Andrei N Baranov

J. Phys. Chem. C, **Just Accepted Manuscript** • DOI: 10.1021/acs.jpcc.9b05762 • Publication Date (Web): 31 Jul 2019

is published by the American Chemical Society. 1155 Sixteenth Street N.W., Washington, DC 20036

Creation of Acceptor Centers in ZnO Single Crystals by Annealing in Sb Vapor

Nikolai O. Taibarei[a], Vladimir G. Kytin[b,d], Eugenii E. Kupriyanov[b], Vladimir A. Kulbachinskii[b,e], Maksim A. Makhiboroda[c], Andrei N. Baranov[a,*]

a. Lomonosov Moscow State University, Department of Chemistry, Leninskie Gory 1, bld. 3, 119991, Moscow, Russia.

b. Lomonosov Moscow State University, Faculty of Physics, Leninskie Gory, bld. 2, 119991, Moscow, Russia.

c. National Research University of Electronic Technology (MIET), Shokin Square, bld. 1, Zelenograd, Moscow, Russia, 124498.

d. VNIIFTRI, Mendeleevo, Moscow region, Russia, 141570

e. Moscow Institute of Physics and Technology (State University) 141700 Dolgoprudny, Moscow Region, Russia

The work was conducted in Lomonosov Moscow State University, GSP-1, Leninskie Gory, Moscow, 119991, Russian Federation

*Corresponding author contacts:

tel: +7 (495) 939-10-83

e-mail: anb@inorg.chem.msu.ru

Abstract

We have investigated the influence of Sb on the carrier concentration of ZnO single crystals. ZnO single crystal substrates were doped in a sealed ampule by annealing in the Sb vapor at temperatures from 700 to 900°C in order to create acceptor centers in ZnO. The dopant concentration profiles were determined by secondary ion mass spectrometry. A significant distinction in dopant concentrations as well as depth of penetration was observed for different temperatures of annealing. Electrical properties of the samples were studied by Hall Effect and resistivity measurements. Valence states of Sb in the samples were investigated by XPS method to prove incorporation of the latter in the matrix of ZnO before and after oxygen annealing. The evolution of the carrier concentration of ZnO along with the valence state of Sb is explained.

Introduction

ZnO is a promising material for ultraviolet light-emitting diodes, laser diodes with low thresholds[1,2] and photodetectors due to its physical properties, such as a wide band gap of 3.37 eV and a large exciton binding energy of 60 meV at room temperature.[3-5] Non-doped ZnO exhibits an n-type semiconductor behavior, which is considered to be provided by certain native point defects (oxygen vacancies (V_O) and interstitial zinc (Zn_i) or hydrogen impurities[6] according to the common accepted point of view.[7] The fabrication of stable and reproducible p-type ZnO has been difficult due to the self-compensation, the low solubility of the acceptor dopants (typically $<10^{18}$ cm^{-3}) and the large ionization energy (170–380 meV) of all the probable acceptor dopants.[8-11] Recently, there have been a number of reports on the obtaining of p-type ZnO through doping by elements of the V group such as N,[12,13] P,[14] As,[15] and Sb[16]. In these works, samples of doped ZnO were obtained as thin films by CVD/MOCVD in the case of N and As doping, radio-frequency sputtering in the case of P and molecular beam epitaxy in the case of Sb. While nitrogen has been regarded as the most suitable dopant for the obtaining of p-type conductivity in ZnO due to the similarity between atomic radii of nitrogen and oxygen, numerous experiments have displayed that it is difficult to prepare stable and reproducible p-type ZnO by N-doping. Moreover, it was reported that N is a deep acceptor in ZnO with high ionization energy of 1.3 eV.[17]

Based on first-principles calculations, Limpijumnong et al.[18] proposed a model for doping by large-size-mismatched Impurities. According to this theory, the Sb atom does not simply substitute on the oxygen position, but rather occupies the Zn sites (Sb_{Zn}) in ZnO. Each Sb atom has sufficient energy to spontaneously induce two zinc vacancies (V_{Zn}), forming a shallow multicharge acceptor complex Sb_{Zn}-$2V_{Zn}$ with a formation energy $\Delta H_f(0)$ = 2.0 eV and acceptor ionization energies $\varepsilon(0/-)$ = 0.16 eV and $\varepsilon(-/3-)$ = 1.37 eV. A direct evidence of Sb occupying Zn sites in ZnO by using the emission channeling technique was explained by Wahl et al.[19] There have been a variety of works exploiting this idea in order to obtain Sb-doped ZnO films by applying different but relative techniques such as molecular beam epitaxy,[20] pulsed laser deposition,[21] radio-frequency sputtering,[22] and dual ion beam sputtering deposition.[23] However the results were controversial and the films had diverse characteristics and properties with poor stabilities. As for ZnO single crystal doped with Sb there only a few reports concerning this system.[24] In that work ZnO single crystals were doped during hydrothermal growth using Sb_2O_3, Sb_2O_5 and $K(SbO)C_4H_4O_6 \cdot 3H_2O$ as the sources of Sb. All samples exhibited n-type conductivity with electron concentrations up to $7 \cdot 10^{17}$ cm^{-3}.

We propose a simple technique for doping of ZnO with antimony by annealing of ZnO single crystal substrates in a Sb vapor and examine transport properties of Sb-doped ZnO single crystals.

Experimental

As starting materials hydrothermally grown ZnO single crystal substrates (orientation <0001>, width ~ 0.5 mm) were taken from "Mineral" Lmtd. (Alexandrov, Russia). Pieces of substrates were sealed inside vacuumed quartz ampules (residual pressure < 0.1 mbar) together with the powder of Sb metal (of 99.999% purity) and then annealed in a tube furnace from 24 h up to 1 week at 700, 800 and 900°C. After that substrates were recovered and heated at 650°C in a Ar flow reactor with a dynamic vacuum system for 30 min in order to remove excess of Sb from the surface of the samples. Some of the samples were later annealed in oxygen-rich atmosphere (a mixture of oxygen and argon in the ratio of 1:3 at a flow rate of 170 sccm) for 1 h in order to activate acceptor centers.

Hall Effect and resistivity were measured by 4-probe method. Typical size of the samples was 2.5x4x0.5 mm. Contacts to the samples were made from In-Pb-Sn alloy. Hall Effect was measured at room temperature and at 77 K in magnetic fields up to 0.7 T. Hall effect was used to determine the conductivity type, concentration of carriers and their mobility.

Evolution of valence states of Sb in the matrix of ZnO upon doping and following annealing at various atmospheres was revealed by X-ray photoelectron spectroscopy (XPS) using PHI VersaProbe II 5000. Calibration was performed by the Au4f (84.0 eV) and Cu2p3 (932.6 eV) lines. Monochromatic Al Kα radiation (hν = 1486.6 eV) with the power of 50 W was used as an excitation source. The spectra were recorded with a resolution of 0.1 eV. X-ray diffraction (XRD) patterns were collected at X-ray diffractometer Rigaku D/MAX-2500V/PC with rotation anode and CuKα1 radiation (λ = 0.15418 nm, scan step size of 0.02°).

The doping depth profiles of the samples were studied by secondary ion mass spectrometry (SIMS) on a Time-of-Flight mass spectrometer ToF.SIMS 5–100 by ION-TOF. The energy of the Bi^+ beam was 30 keV. $^{133}Cs^+$ with energy of 2 keV was used as the primary ion. A Bruker EDX spectrometer was used for quantitative elemental analysis at different depths of the samples.

Results and discussion

The doped samples annealed at temperatures of 700, 800 and 900°C were marked as ZSC700, ZSC800 and ZSC900 respectively and non-doped ZnO single crystals annealed at 900°C as ZSCP.

The SIMS method was applied in order to determine the distribution of Sb in the samples. The profiles from the SIMS analysis for ZSC700 and ZSC800 are presented in figure 1. As it can be seen, except the initial kink that can be attributed to the surface of the samples a relatively fast drop of Sb content takes place as diffusion limits the ability of Sb to penetrate into the bulk of the samples. The maximum depth, where Sb can be detected by EDX, was found to be about 3 μm for ZSC700. This value is significantly smaller for ZSC800 (about 650 nm). And there was almost no Sb found in ZSC900 deeper than at 100 nm (where its

concentration was 2.46 wt%), which is why its graph is not shown here. This dependence of the maximum depth of penetration on annealing temperature can be explained by evaporation of the superficial layer of ZnO single crystals during annealing in accordance with the following reaction that takes place upon temperature increase[25]:

$$2ZnO_{(s)} \rightarrow 2Zn_{(g)} + O_{2(g)}$$

In the case of lower temperatures the rate of evaporation is much lower than the rate of diffusion into the bulk. But as temperature goes up to 900°C, the rates of evaporation and diffusion are almost equalized and thus only very thin superficial layer of ZnO is doped with Sb.

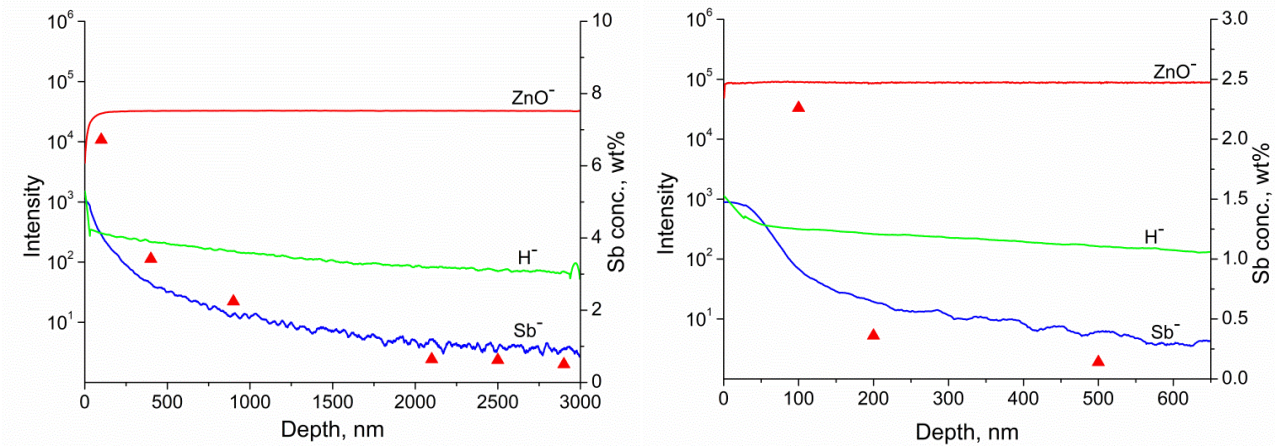

Figure 1
Depth concentration profiles of Sb and H for ZSC700 (left) and ZSC800 (right) with concentrations of Sb at different levels (red triangles).

The most abundant impurity element except Sb in the samples that is most likely embedded in the structure of ZnO during hydrothermal growth of single crystal in aqueous media is hydrogen, which is known to act as a donor. Its content is approximately independent on the depth and decreases slowly in deeper layers. There was also found some unavoidable contamination by carbon deposited from the atmosphere on the surface of the samples and a rather small but detectable content of Na probably transferred to the samples from alkali aqueous media used for the growth of ZnO single crystal.

The main oxidation states of Sb are known to be +3 and +5. In the case of p-type doping of ZnO the Sb_{Zn}-$2V_{Zn}$ acceptor complex contains Sb^{+5} so it is important to know that Sb actually reaches its highest oxidation state, otherwise it will act as a donor. There is almost no information presented in the literature concerning what oxidation state Sb has being inserted in the matrix of ZnO. At the initial stage of annealing antimony in a vapor has Sb^0 oxidation state. One may suggest that the only oxidizing agent available in the closed system was Zn^{2+}, which can potentially oxidize Sb by the following red-ox reaction:

$$Zn^{2+}_{(s)} + \frac{2}{x}Sb^{0}_{(g)} \rightarrow Zn^{0}_{(g)} + \frac{2}{x}Sb^{x+}_{(s)}$$

Consequently, XPS was applied to determine the oxidation state of Sb in our samples. Figure 2 displays a typical XPS spectrum of the samples annealed at 700-900°C. For the other samples the spectra did not change significantly so they are not shown here. The $Sb3d_{3/2}$ transition peak corresponds to Sb(V) and no Sb(III) contribution can be found. The larger peak can be deconvoluted into contributions of $Sb3d_{5/2}$ and O1s. $Sb3d_{5/2}$ position is constrained based on the energy difference between $Sb3d_{3/2}$ and $Sb3d_{5/2}$ that equals to ~9.4 eV and the cross-sectional ratio, which is 1.45[26,27]. The maximum appears at 541 eV, which is 0.9 eV higher than 540.1 eV given in the literature data. This shift is due to charging of the sample during the analysis and can be determined from C1s peak shift of adventitious carbon on the same sample. In our case, this shift was ~1 eV which is in good agreement with the position of the other peaks. It is worth mentioning that no metallic antimony was found here. It means that excess antimony was completely removed during the vacuuming after the synthesis. Consequently, we can propose that all antimony in the samples is actually integrated in the structure of ZnO and not just deposited on the surface from the Sb vapor. Formation of Sb_{Zn}-$2V_{Zn}$ with low $\Delta H_f(0)$ = 2.0 eV favors oxidation of Sb^0 to Sb^{+5} by Zn^{2+}, which otherwise would be impossible due to Zn^0 being a stronger reducing agent than Sb^0.

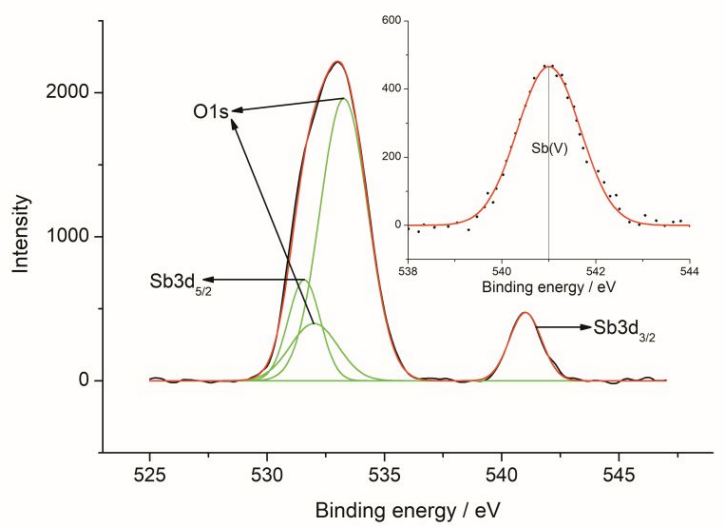

Figure 2
A typical XPS spectrum of Sb-doped single crystals. Black lines and dotes denote experimental data, green and red lines are the result of digital optimizations. The insertion displays the Sb 3d3/2 peak.

As well known, annealing in oxygen atmosphere previously was used to activate Sb as an acceptor since it was suggested that such conditions are responsible for the formation of the Sb_{Zn}-$2V_{Zn}$ acceptor complex[23]. Our samples were doped in an oxygen-free atmosphere. So we checked what will happen with the samples after annealing in an oxygen-rich atmosphere. After 1 h annealing in oxygen at 650°C the samples have lost their conducting properties. The resistance has increased from 10-100 Ω to tens MΩ so it was not possible to carry out Hall measurements for the samples after such a treatment. Figure 3 shows the XPS spectrum of the same sample after annealing in oxidizing atmosphere. Since the sample had very low

conductivity, a discharging electron beam was applied for charge compensation when recording the spectra. That resulted in a shift of peaks towards lower energies. This shift was derived from the position of the C1s peak and was found to be –1.8 eV. Taking into account the shift, the position of the two peaks precisely matches with the binding energies for pure Sb_2O_4[26]. While it is hard to deconvolute the $Sb3d_{3/2}$ peak into contributions of Sb(III) and Sb(V), the other peak can still be deconvoluted into the $Sb3d_{5/2}$ and O1s lines.

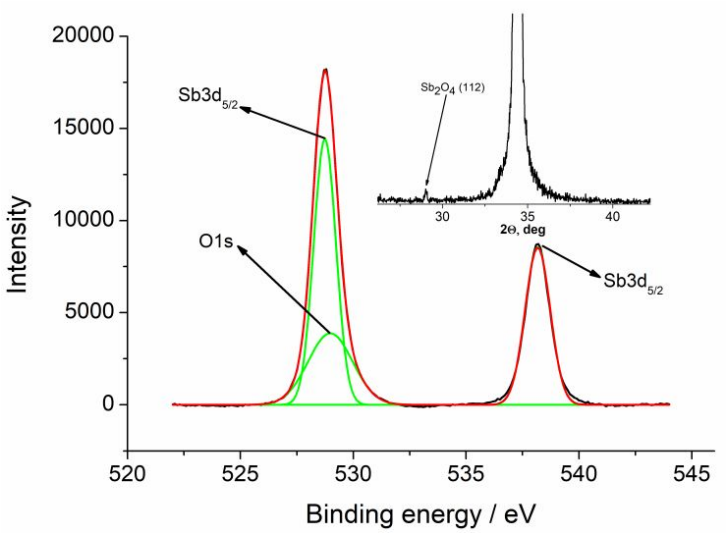

Figure 3

The XPS spectrum of an oxygen-annealed Sb-doped single crystal. Black lines denote experimental data, green and red lines are the result of digital optimizations. The inset shows the XRD pattern of an oxygen-annealed Sb-doped single crystal.

The presence of Sb_2O_4 was also confirmed by XRD analysis. The inset in figure 3 gives the XRD pattern of the same sample. The strongest (112) peak of Sb_2O_4 can be clearly observed at 29.0° even though it has a very low intensity compared to (002) and (004) peaks of monocrystalline ZnO. Besides that, no other phases were found. To an extent, Sb_2O_4 phase could be seen with the naked eye on the surface of the annealed substrates, which means that annealing leads to precipitation of the dopant from single crystals.[28]

The fact that antimony lowers its oxidation state during high temperature oxidative annealing might seem contradictory at the first look. However, it can be easily explained if we consider that temperature treatment could lead to “self-cleaning” of single crystals while it is known that Sb_2O_5 tends to decompose into lower oxides upon temperature increase with β-Sb_2O_4 being the final product at temperature higher than 900°C.[29] In our case this process occures at lower temperature of 650°C, which is probably due to ambient pressure in the reactor being substantialy lower than atmospheric. Strong decrease of conductivity during annealing in oxygen reach atmosphere can be explained by the reduction of concentration of donors. Thus, we established that while it is important to reach Sb^{+5} oxidation state, using oxygen for that purpose at high temperature of annealing as it was proposed previously might be inappropriate due to formation and precipitation of Sb_2O_4.[18]

The transport properties of the samples were studied by 4-probe method. According to Hall Effect measurements at room temperature and at 77 K, all samples exhibit n-type conductivity. The dependence of Hall resistivity on magnetic field was linear in magnetic field up to 0.7 T. Electron concentration n and mobility μ were calculated using expressions valid for a one group of carriers:

$$n = \frac{1}{ed\partial\rho_{xy}/\partial B}; \mu = {}^{1}/_{e\rho_{xx}n} \quad (1)$$

where *e* is the elementary charge, *d* is the thickness of the sample, ρ_{xx} and ρ_{xy} are the resistivity and the Hall resistivity, *B* is the magnetic induction.

The product of electron wave number k_T corresponding to thermal energy and electron mean free path *l* was estimated to check the electron transport mechanism using following expression:

$$k_T l = \frac{2k_B Tm\mu}{e\hbar} \quad (2)$$

where k_B is the Boltzmann constant, *T* is the temperature, *m* is the electron effective mass, $\hbar$ is the Planck constant.

The product $k_T l$ is significantly larger than unity for all samples at room temperature and also larger than unity at 77 K. This corresponds to the electron transport in conduction band and confirms the applicability of expression (1). The results of Hall measurements are given in Table 1.

Table 1
Electron concentrations, mobilities and product kTl determined from Hall measurements at room temperature and at 77 K for the samples annealed at different temperatures.

Sample	Annealing temperature, °C	Hall electron concentration, 10^{15} cm^{-3} at 295 K	Hall electron concentration, 10^{15} cm^{-3} at 77 K	Mobility, $cm^2/(V·s)$ at 295 K	Mobility, $cm^2/(V·s)$ at 77 K	$k_T l$ at 295 K	$k_T l$ at 77 K
ZSC700	700	3.6	0.55	75	64	5.9	1,3
ZSC800	800	15	0.96	92	91	7.2	1,8
ZSC900	900	30	2.3	63	150	4.9	3
ZSCP (Undoped ZnO)	900	260	10	160	860	12	17

A clear dependence of electron concentration on annealing temperature can be seen. Temperature dependence of resistivity of the samples is shown in figure 4. At low temperatures resistivity of all samples increases with the decrease of temperature. Hall Effect measurements at 77 K also yield much lower electron concentration at 77 K than at room temperature. This indicates that mobile electrons freeze on defects and impurities. Temperature dependence of resistivity of non-doped sample exhibits minimum near 200 K and metallic type of dependence at temperature above 200 K. This is usually observed in case of

ionization of majority of donors and can be used to estimate concentration of donors assuming it equal to the concentration of electrons at room temperature, i.e 2,6 10^{17} cm^{-3}.

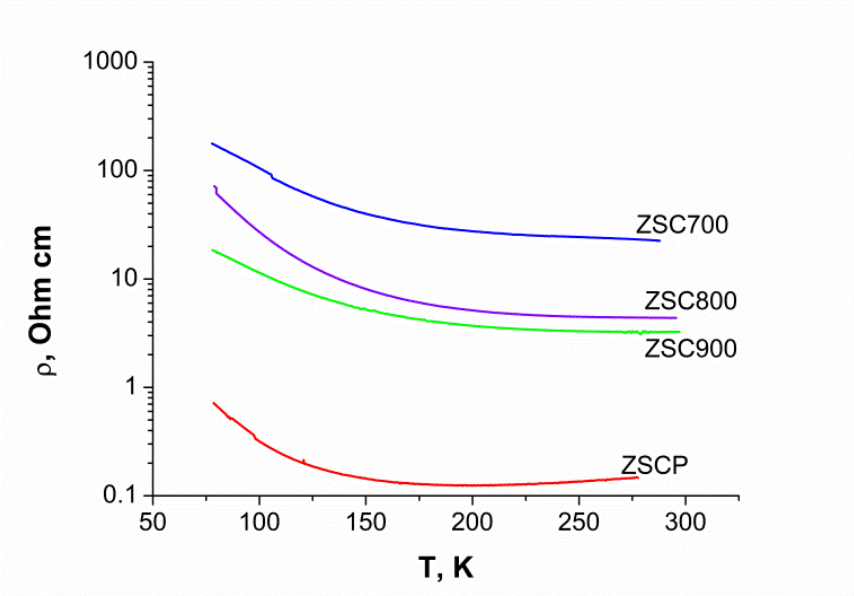

Figure 4

Temperature dependencies of resistivity of the samples.

The concentration of electrons increases as annealing temperature increases for the samples annealed for the same amount of time (24 h). High temperature treatment in oxygen deficit atmosphere creates native point defects in ZnO as discussed earlier, which serve as donors. Also there are less acceptor centers formed at higher temperatures since the ultimate depth of penetration of Sb atoms decreases dramatically. The highest electron concentration as well as the highest mobility was observed in the sample that is non-doped ZnO after the same temperature treatment. We suggest that the drop of carrier concentrations and mobilities in Sb-doped samples compared to non-doped ZnO is due to formation of acceptor centers, which partially compensate for native donors but cannot overcome their cumulative effect because of the insufficient quantity and low depth of penetration.

Conclusions

A new technique was successfully applied for Sb doping of single crystal ZnO by annealing in the Sb vapor. The concentration of Sb in the samples demonstrates a strong dependence on annealing temperature and tends to decrease as temperature increases from 700 to 900°C along with the maximum depth of penetration. The electron concentrations were found to range from $3.6 \cdot 10^{15}$ cm^{-3} at 700°C to $3 \cdot 10^{16}$ cm^{-3} at 900°C because high temperature treatment supports creation of native point defects in ZnO and impedes formation of acceptor centers. We also confirmed that acceptor properties are caused by Sb(V) as

it was predicted even though the use of oxygen-rich annealing conditions can lead to precipitation of the dopant. The described simple technique can be potentially used for doping ZnO thin films and some nanostructures like ZnO nanorods.

Acknowledgements

The work was partially (MMA personally) supported by the Minobrnauki RF (Goszadanie № 16.2475.2017/4.6) and VIMS measurements were performed using the equipment of MIET Core facilities center "MEMS and electronic components", MIET Center for National Technology Initiative (NTI) “Sensory”. The authors are grateful to “Mineral” Ltd. Company and personally to M.A. Arkhipov for providing the ZnO substrates.

References

(1) Choopun S.; Vispute R. D.; Noch W.; Balsamo A.; Sharma R. P.; Venkatesan T. Oxygen Pressure-Tuned Epitaxy and Optoelectronic Properties of Laser-Deposited ZnO Films On Sapphire. *Appl. Phys. Lett*. **1999**, *75*, 3947-3949.

(2) Ko H. J.; Chen Y. F.; Zhu Z.; Yao T. Photoluminescence Properties of ZnO Epilayers Grown on CaF_2(111) by Plasma Assisted Molecular Beam Epitaxy. *Appl. Phys. Lett*. **2000**, *76*, 1905-1907.

(3) Wong E. M.; Searson P. C. ZnO Quantum Particle Thin Films Fabricated by Electrophoretic Deposition. *Appl. Phys. Lett*. **1999**, *74*, 2939-2941.

(4) Yu P.; Tang Z. K.; Wong G. K. L.; Kawasaki M.; Ohtomo A.; Koinuma H.; Segawa Y. Room-Temperature Gain Spectra and Lasing in Microcrystalline ZnO Thin Films. *J. Cryst. Growth* **1998**, *184–185*, 601-604.

(5) Bagnall D. M.; Chen Y. F.; Zhu Z.; Yao T. Optically Pumped Lasing of ZnO at Room Temperature. *Appl. Phys. Lett*. **1997**, *70*, 2230-2232.

(6) Janotti A.; Van de Walle C. G. Native Point Defects in ZnO. *Phys. Rev. B*. **2007**, *76*, 165202.

(7) Zhang S. B.; Wei S.-H.; Zunger A. Intrinsic n-Type versus *p*-Type Doping Asymmetry and the Defect Physics of ZnO. *Phys. Rev. B* **2001**, *63*, 075205.

(8) Li J.; Wei S.-H.; Li S.-S.; Xia J.-B. Design of Shallow Acceptors in ZnO: First-Principles Band-Structure Calculations. *Phys. Rev. B* **2006**, *74*, 081201(R).

(9) Puchala B.; Morgan D. Stable Interstitial Dopant-Vacancy Complexes in ZnO. *Phys. Rev. B* **2012**, *85*, 195207.

(10) Avrutin V.; Silversmith D. J.; Morkoc H. Doping Asymmetry Problem in ZnO: Current Status and Outlook. *Proceedings of the IEEE* **2010**, *98(7)*, 1269-1280.

(11) Yan Y.; Li J.; Wei S.-H.; Al-Jassim M. M. Possible Approach to Overcome the Doping Asymmetry in Wideband Gap Semiconductors. *Phys. Rev. Lett*. **2007**, *98*, 135506.

(12) Minegishi K.; Koiwai Y.; Kikuchi Y.; Yano K.; Kasuga M.; Shimizu A. Growth of *p*-Type Zinc Oxide Films by Chemical Vapor Deposition. *Jpn. J. Appl. Phys*. **1997**, *36*, L1453-L1455.

(13) Jianfeng S.; Chunjuan T.; Qiang N.; Changqing W.; Zhuxi F. Variation of N Acceptor Energy Induced by Al-N Codoping in ZnO Films. *J. of Alloys and Compounds* **2010**, *500(1)*, 5-8.

(14) Kim K.-K.; Kim H.-S.; Hwang D.-K.; Lim J.-H.; Park S.-J. Realization of *p*-Type ZnO Thin Films via Phosphorus Doping and Thermal Activation of the Dopant. *Appl. Phys. Lett*. **2003**, *83*, 63-65.

(15) Huang Y.-C.; Weng L.-W.; Uen W.-Y.; Lan S.-M.; Li Z.-Y.; Liao S.-M.; Lin T.-Y.; Yang T.-N. Annealing Effects on the *p*-Type ZnO Films Fabricated on GaAs Substrate by Atmospheric Pressure Metal Organic Chemical Vapor Deposition. *J. Alloys Compd.* **2011**, *509(5)*, 1980-1983.

(16) Yang Z.; Chu S.; Chen W. V.; Li L.; Kong J.; Ren J.; Yu P. K. L.; Liu J. ZnO:Sb/ZnO:Ga Light Emitting Diode on c-Plane Sapphire by Molecular Beam Epitaxy. *Appl. Phys. Express* **2010**, *3*, 032101.

(17) Lyons J. L.; Janotti A.; Van de Walle C. G. Why Nitrogen Cannot Lead to *p*-Type Conductivity in ZnO. *Appl. Phys. Lett*. **2009**, *95*, 252105.

(18) Limpijumnong S.; Zhang S. B.; Wei S.-H.; Park C. H. Doping by Large-Size-Mismatched Impurities: the Microscopic Origin of Arsenic- or Antimony-Doped *p*-Type Zinc Oxide. *Phys. Rev. Lett*. **2004**, *92*, 155504.

(19) Wahl U.; Correia J. G.; Mendonça T.; Decoster S. Direct Evidence for Sb as a Zn Site Impurity in ZnO. *Appl. Phys. Lett*. **2009**, *94*, 261901.

(20) Xiu F. X.; Yang Z.; Mandalapu L. J.; Zhao D. T.; Liu J. L. High-Mobility Sb-Doped *p*-Type ZnO by Molecular-Beam Epitaxy. *Appl. Phys. Lett*. **2005**, *87*, 152101.

(21) Guo W.; Allenic A.; Chen Y. B.; Pan X. Q. Microstructure and Properties of Epitaxial Antimony-Doped *p*-Type ZnO Films Fabricated by Pulsed Laser Deposition. *Appl. Phys. Lett*. **2007**, *90*, 242108.

(22) Wang P.; Chen N.; Yin Z.; Yang F.; Peng C. Fabrication and Properties of Sb-Doped ZnO Thin Films Grown by Radio Frequency (RF) Magnetron Sputtering. *J. Cryst. Growth* **2006**, *290(1)*, 56-60.

(23) Pandey Sushil K.; Pandey Saurabh K.; Awasthi V.; Gupta M.; Deshpande U. P.; Mukherjee S. Influence of *in-situ* Annealing Ambient on *p*-Type Conduction in Dual Ion Beam Sputtered Sb-Doped ZnO Thin Films. *Appl. Phys. Lett*. **2013**, *103*, 072109.

(24) Grossner U.; Christensen J. S.; Svensson B. G.; Kuznetsov A. Yu. Carrier Concentration and Shallow Electron States in Sb-Doped Hydrothermally Grown ZnO. *Superlattices Microst.* **2007**, *42(1-6)*, 294-298.

(25) Secco E. A. Decomposition of Zinc Oxide. *Can. J. Chem.* **1960**, *38(4)*, 596-601.

(26) Garbassi F. XPS and AES Study of Antimony Oxides. Surf. Interface Anal. **1980**, *2(5)*, 165-169.

(27) Scofield J. H. Hartree-Slater Subshell Photoionization Cross-Sections at 1254 and 1487 eV. *J Electron. Spectrosc. Relat. Phenomena* **1976**, *8(2)*, 129-137.

(28) Rita E.; Alves E.; Wahl U.; Correia J. G.; Monteiro T.; Soares M. J.; Neves A.; Peres M. Stability and Luminescence Studies of Tm and Er Implanted ZnO Single Crystals. *Nucl. Instrum. Methods. Phys. Res. B* **2006**, *242(1-2)*, 580-584.

(29) Stewart D. J.; Knop O.; Ayasse C. Pyrochlores. VII. The Oxides of Antimony: an X-Ray and Mössbauer Study. *Can. J. Chem.* **1972**, *50(5)*, 690-700.

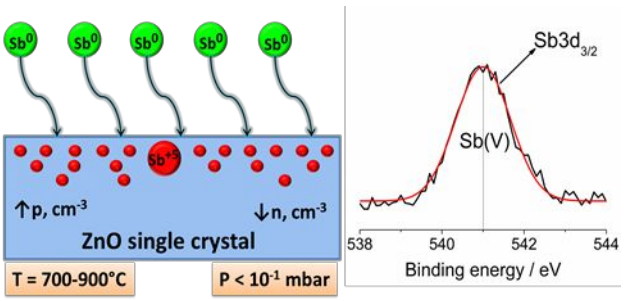
Sb0
Sb0
Sb0
Sb0
Sb0
Sb+3
↑p, cm-3
↓n, cm-3
ZnO single crystal
T = 700-900°C
P < 10-1 mbar
Sb3d3/2
Sb(V)
538
540
542
544
Binding energy / eV

TOC Graphic.